Magnetic hardening mechanisms in Nd-Fe-B nanocrystalline material

M. T. Clavaguera-Mora and J. A. Diego
Grup de Física de Materials, Facultat de Ciéncies, Universitat Autònoma de Barcelona, 08193-Bellaterra, Spain

N. Clavaguera
Departamento Estructura i Constituents de la Matèria, Facultat de Física, Universitat de Barcelona, Diagonal 647, 08028-Barcelona, Spain

A. Hernando and M. Vázquez[a)]
Instituto de Magnetismo Aplicado RENFE-Universidad Complutense, Apdo. 155 Las Rozas, 28230 Madrid, Spain

(Received 16 August 1993; accepted for publication 18 March 1994)

Microstructural and magnetic measurements of the evolution by heat treatment of initially amorphous $Nd_{16}Fe_{76}B_8$ alloys prepared by melt spinning are presented. Evidence of magnetic hardening above a threshold temperature induced by magnetic isolation of the $Nd_2Fe_{14}B$ grains is provided. A thermodynamic and kinetic explanation of local melting of the intergranular nanostructured Nd-rich eutectic phase at temperatures below 900 K based on capillary effects is presented. A subsequent Ostwald ripening process moves Nd to wet intimately the hard magnetic grains, becoming, on cooling, a real paramagnetic isolating thin film (~2.5 nm). By using a simple analogy, it is shown that the switching magnetization field in a single-domain crystal can be drastically affected through the exchange coupling to neighboring grains with different orientation of the easy axis. This effect should be important enough to reinforce the coercive field of polycrystalline hard magnetic materials and explains the observed enhancement from 0.9 to 1.9 T.

I. INTRODUCTION

Magnetic hardening by crystallization in overquenched NdFeB ribbons is well known, however, the increase of coercivity by crystallization of fully amorphous samples and the mechanisms through which this is accomplished are much less studied subjects. The fine-grained microstructure and the appearance of a Nd-rich phase located at the grain boundaries of the $Nd_2Fe_{14}B$ (ϕ) hard magnetic phase have been proposed as the main factors promoting superior magnetic properties in rapidly solidified alloys.[1] Such microstructures have been obtained either by controlled direct quench or by annealing the overquenched material.[2,3] An important effort has been devoted to crystallization kinetic studies focused to the design of the optimal heat treatment conditions needed to obtain the correct size and distribution of the hard magnetic phase.[4–7]

A decisive step in the coercivity enhancement of melt-quenched NdFeB material is a heat treatment at 870–920 K.[8–12] Such annealing may duplicate the coercive values of optimum direct-quenched materials. However, a clear understanding of the mechanisms which lead to coercivity enhancement by the direct amorphous cast/annealing route is of vital importance for the future development of fully dense NdFeB permanent magnets from melt-quenched ribbons.

The aim of this article is the study of microstructural, thermodynamic, and kinetic factors which promote magnetic hardening by a suitable heat treatment and to analyze the underlying mechanisms. For that purpose the evolution of both microstructure and magnetic behavior as a function of the degree of crystallization and annealing procedure has been undertaken. The coercivity and magnetization process for samples annealed at several different temperatures are discussed considering the influence of the exchange coupling between neighboring grains having uniaxial anisotropy and different easy axes.

II. EXPERIMENT

Master alloys of nominal composition $Nd_{16}Fe_{76}B_8$ were provided by Gesellschaft für Elektrometallurgie, Nürnberg. Melt-spun amorphous alloys were obtained by quenching the molten material on the surface of a rapidly spinning cooper wheel in helium atmosphere. The amorphous material was annealed at different temperatures and different times under Ar atmosphere in order to study the relationship between heat treatment, microstructure, and magnetic properties. Microstructural observations were carried out with a transmission electron microscope (TEM), Hitachi H-800 (200 kV) on thin foils prepared by Ar-ion-beam thinning and on a scanning electron microscope (SEM), Hitachi S-570, on fresh fractured surfaces. Magnetic measurements were performed with a superconducting quantum interference device (SQUID) magnetometer (Quantum Design).

It is of relevant importance for the proposed study to obtain the material in a really amorphous state in order to avoid the influence on the crystallization behavior of preexisting nuclei. Taking in account the multiple factors that influence the real cooling rate in the melt spinning process, a complete characterization of the as prepared samples is necessary to assure their amorphous state and homogeneity. For wheel surface velocities of 40 m/s or above an amorphous material was obtained, characterized by fresh fractured sur-

[a)]Permanent address: Instituto de Ciencia de Materiales, Serrano 144, 28006 Madrid, Spain.

 0021-8979/94/76(2)/1124/7/$6.00

faces with the typical glass concoidal structure, a diffuse maximum in the x-ray- and electronic-diffraction patterns, and the absence of any coercive volume fraction of the material (associated with as quenched ϕ crystals).

III. MICROSTRUCTURAL AND MAGNETIC EVOLUTION WITH THE HEAT TREATMENT

The crystallization of amorphous $Nd_{16}Fe_{76}B_8$ may be fully achieved either by heating in a temperature interval which depends on the heating rate (typically between 880 and 920 K for heating rates up to 320 K/min) or by annealing during a time interval which depends on the annealing temperature (typically 10 min at 820 K). A systematic study of the evolution of the microstructure with heat treatment and of its influence in the magnetic properties has been undertaken.

A. Isothermal annealing at temperatures in the range 755–850 K

Different degrees of crystallization have been obtained annealing the material at 795 K for time intervals up to 165 min and at 755 K up to 900 min (full crystallization is achieved at both temperatures). Any crystallization previous to these isothermal annealings has been avoided heating up the samples at high heating rate (320 K/min). The same evolution of the microstructure is observed in both cases, with only a slow-down-time scale for the samples annealed at 755 K compared to those annealed at 795 K.

The crystallization process shows two differentiated stages. During the first stage, crystallization takes place via the nucleation of nanocrystals of the ϕ phase, which, on further annealing, grow equiaxially and simultaneously with the nucleation of new crystals as shown in Fig. 1(a) for a sample annealed 20 min at 795 K. When the crystalline fraction of the material reaches the value of about 60%, i.e., after annealing 360 min at 755 K or 24 min at 795 K, a secondary crystallization of quite small nanocrystals (size ~10 nm) occurs around some primary ϕ grains [Fig. 1(b)]. There is no significant change in the size of these small nanocrystals on further annealing at these temperatures. Fully crystalline samples show ϕ grains, with sizes up to 500 nm and very irregular borders, mostly surrounded by the small crystals resulting from the secondary crystallization. That is, secondary crystallization produces a very refined nanostructured intergranular phase, and is probably driven by a decrease in Fe content on the amorphous boundary layer ahead of the interface of ϕ grains.[13] Any attempt to analyze the nature of this intergranular phase was unsuccessful, however, they most probably correspond to the eutectic crystallization of ϕ-$Nd_{1+\epsilon}Fe_4B_4$(η)-Nd, as is discussed later. X-ray-diffraction patterns on these samples show some evidence of η Bragg peaks, apart from those of the ϕ phase, although is is not possible to clearly detect the presence of crystalline Nd because most of its reflections overlap with Bragg peaks of the ϕ phase. The same microstructure is obtained when the samples are annealed at temperatures in the range 825–850 K, as has been reported previously.[14]

Samples fully crystallized at temperatures in the range 755–850 show very similar magnetic properties, with coercive fields which do not exceed 1 T. Figure 2 reproduces the hysteresis loop corresponding to a sample annealed 15 min at 850 K.

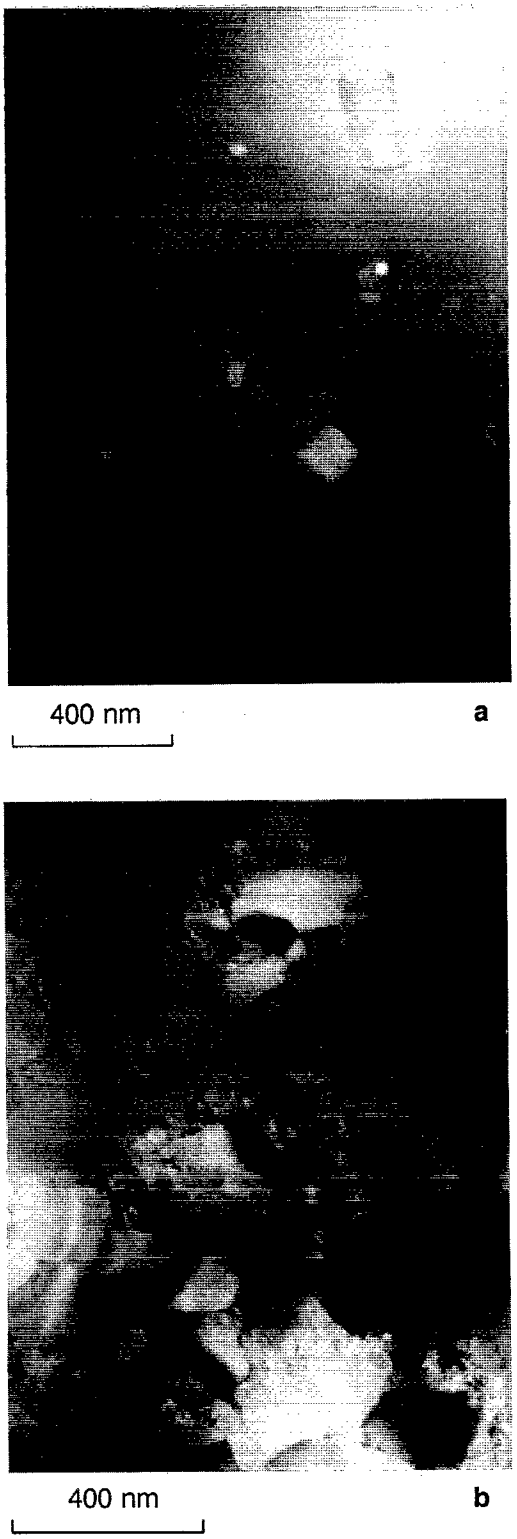

FIG. 1. Microstructure of samples with different degree of crystallization after annealing at 795 K for (a) 20 min (α~30%) and (b) 24 min (α~60%). The arrow indicates the secondary nanostructured crystallization of $Nd_2Fe_{14}B$-$Nd_{1+\epsilon}Fe_4B_4$-Nd.

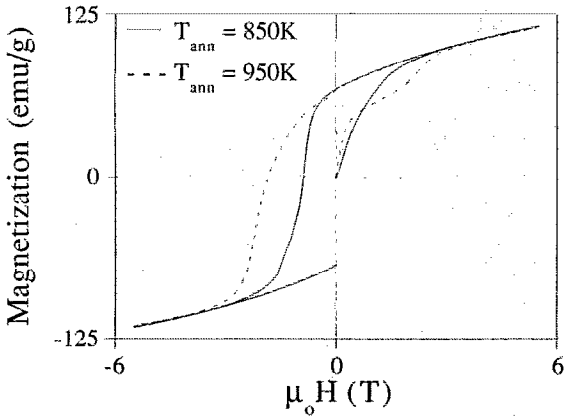

FIG. 2. Hysteresis loops corresponding to the samples annealed at 850 and 950 K during 15 min.

B. Influence of annealing at temperatures in the range 900–1000 K

Another microstructure is obtained when the amorphous samples are annealed at temperatures in the range 900–1000 K. Fully crystalline samples have ϕ crystals which show approximately the same size, but smoother surfaces than those obtained when annealing at 755–850 K, and a very thin (~2.5 nm) continuous film in between the ϕ grains. According to the starting composition of the alloy (near that of sintered magnets) and the processing conditions (heat treatment of the amorphous sample), the thin-film intergranular phase must be a Nd phase, similar to those reported for sintered magnets,[15] rather than the Nd-Fe eutectic phase ($Nd_{70}Fe_{30}$) usually found for low boron content alloys directly obtained as nanocrystalline by rapid solidification.[16]

The microstructure obtained can result not only by direct annealing of the fully amorphous alloy at temperatures in the range 900–1000 K but also when the amorphous alloy, already annealed at temperatures in the range 755–850 K, is further heat treated at 900–1000 K. As an example, in Fig. 3 is presented a TEM micrograph of an amorphous sample heated 160 min at 795 K plus 15 min at 950 K.

SEM observations of all the samples heat treated in the range 900–1000 K show also an uniform refinement of the size distribution of the ϕ grains from the wheel surface toward the free surface of the ribbon. Figure 4(a) shows a typical SEM micrograph of a fresh fractured section of a ribbon heat treated 15 min at 950 K.

Samples treated in this range of temperatures (900–1000 K) have coercive fields with values of 1.9 T as observed in Fig. 2. That is, there is an improvement in the magnetic properties (from 1 to 1.9 T) when the range of temperatures of annealing of the amorphous alloy changes from 755–850 to 900–1000 K. Further, the dramatic increase in the coercive field is independent of the previous thermal history of the specimen. Therefore, it must be associated to the change in the microstructure of the interphase because no morphological changes, like grain growth, are detected neither by TEM nor by diffraction techniques.

FIG. 3. Microstructure of the sample treated 160 min at 795 K plus 15 min at 950 K. The arrow indicates the Nd thin-film intergranular phase.

C. Threshold temperature of magnetic improvement

When the initially amorphous alloys are annealed at 875 K TEM observations show that both kinds of intergranular microstructure coexist. Figure 5(a) and 5(b) show two representative micrographs of the overall behavior in the material. As the volume sampled by TEM is extremely small and the exact location of the electron-transparent areas of the thinned foils within the ribbon fragment is not controllable, complementary SEM observations of fresh fractured sections of the ribbons, like that presented in Fig. 4(b), allow us to establish that there is a different location, in the ribbon, of the two kinds of microstructure. The one with the finely nanostructured intergranular phase occurs in the zone of the ribbon near to the wheel surface (this nanostructure cannot be resolved by SEM) while the uniform thin-film intergranular microstructure is located close to its free surface. The hysteresis loop of these ribbons shows a behavior intermediate between that of samples annealed at temperatures in the range 755–850 K and in the range 900–1000 K, in agreement with the microstructural observations.

IV. DISCUSSION

A. Microstructural results

The above-stated microstructural results show clearly that the key of the change in the nature of the intergranular microstructure is related to both the refinement of the crys-

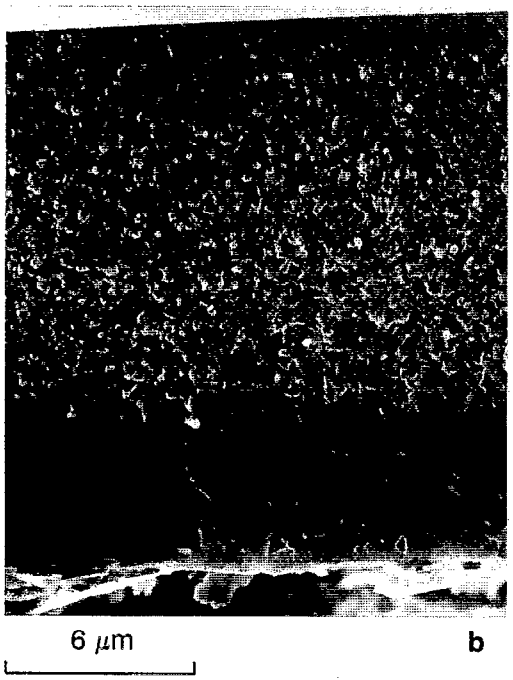

FIG. 4. Cross-section scanning electron micrographs of the samples treated during 15 min at (a) 950 K and (b) 875 K (the arrows in the bottom indicate the part of the material that was in contact with the wheel surface).

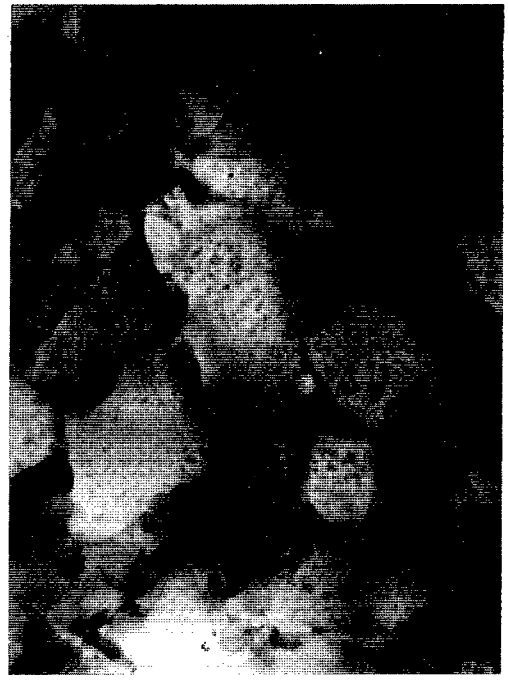

FIG. 5. Representative microstructures present in the sample treated at 775 K during 15 min: (a) nanostructured intergranular phase areas; (b) Nd thin-film intergranular phase areas.

tallized alloy and the anneal temperature. The crucial experiments that are discussed are those obtained for samples annealed at 875 K.

To understand the mechanism responsible for the appearance of a refined crystalline microstructure, attention must be placed in the progress of crystallization related to the nucleation and growth of primary ϕ crystals in the initially amorphous alloy. As it has been shown previously for this materials,[13] we can assume (in a first approximation) an interfacial controlled crystallization with constant nucleation rate and growth of new equiaxial crystals. In this simple case

the total fraction α transformed in the material in isothermal conditions is described by the relation

$$\alpha = 1 - \exp[-(\pi I U^3 t^4)/3], \quad (1)$$

where I is the nucleation frequency of new crystals, U is their growth rate, and t is the time of the heat treatment. The maximum grain size achieved under these conditions is derived simply by the product of the crystal growth rate and the time t_f necessary to almost complete the crystallization (we assume 90%) of the material,

$$r_{\max} = U t_f. \quad (2)$$

From several TEM observations of samples with different degrees of crystallization, heat treated at 795 K, we obtained an estimation of both the nucleation frequency and crystal growth at this temperature. These estimated values are $I=(10\pm5)\times10^{15}$ $m^{-3}\,s^{-1}$ and $U=(10\pm2)\times10^{-11}$ ms^{-1}; however, both I and U are strongly temperature dependent. Therefore, in order to evaluate $r_{\max}$ at 875 K it is necessary to estimate their values at that temperature. By modeling the crystallization kinetics as it has been performed for similar alloys,[17] we obtained $I\sim(10\pm8)\times10^{17}$ $m^{-3}\,s^{-1}$ and $U\sim(3\pm1)\times10^{-9}$ ms^{-1} for the nucleation frequency and crystal growth rate at 875 K. According to these results, the time necessary to almost complete the crystallization at this temperature, derived from Eq. (1), is $t_f\sim90$ s. Equation (2) gives a maximum grain diameter of $d_{\max}=2r_{\max}\sim(580\pm60)$ nm which is very similar to that observed by TEM ($d_{\max}\sim500$ nm) although diffusional processes, very important in the last stages of the crystallization, have been neglected in the modeling. That is, this simple modeling predicts a refined crystalline microstructure which qualitatively agrees with the experimental results.

With regards to the existence of a threshold temperature of magnetic improvement let us make some thermodynamic considerations. According to the published phase diagram,[18] the lowest temperature of melting of a mixture of ϕ, η, and Nd grains is 928 K, which is the temperature of the invariant eutectic equilibrium $L \Leftrightarrow \phi + \eta + \mathrm{Nd}$. However, capillary effects may cause a Gibbs–Thompson undercooling[19] given by $\Delta T = 2\sigma/(r\Delta s)$ where σ is the solid/liquid interface energy, r the radius of curvature, and Δs the melting entropy per unit volume. That is, taking typical values[13,19] for σ and Δs, namely $\sigma=0.1$ $J\,m^{-2}$ and $\Delta s=10^{-6}$ $J\,m^{-3}\,K^{-1}$, the calculated lowest melting temperature for a mixture of ϕ, Δ, and Nd grains with radio of curvature of 4 nm is 878 K, which corresponds to an undercooling of $\Delta T=50$ K.

With this values in mind, the dual microstructure observed in the sample crystallized at 875 K may be explained in the following form. As previously stated, the size of the ϕ grains is much smaller near the wheel surface than at the free surface of the ribbon. When annealing at about 875 K, the highest surface curvatures of the irregular ϕ grains and the most refined nanostructured intergranular phase will occur in areas near the free surface of the ribbon. These zones are those that melt by capillary effects. Once the liquid phase appears, diffusion is promoted and Ostwald ripening phenomenon[19] produces a coarsening of the ϕ and η grains. The remaining Nd liquid, which wets intimately most of the grains, forms, upon cooling a real paramagnetic film which magnetically isolates the grains. Our magnetic measurements confirm this explanation.

B. Schematic description of the influence of the intergranular phase on the coercivity

It has been shown that samples annealed in the range of temperatures from 755 to 850 K exhibit an intergranular nanostructure built up by grains of different phases. These nanometric magnetic particles, when connecting two bigger different grains, play a very important role in determining the shape of the demagnetizing curve, as is outlined below.

In samples annealed at temperatures above 875 K the intergranular region consists of a thin film of a paramagnetic phase. Even though diffraction techniques show a similar distribution of size and orientation of ϕ grains in samples annealed in both ranges of temperature, the coercive force increases from 0.9 to 1.9 T when the annealing is performed at higher temperatures (Fig. 2), i.e., when the intergranular nanostructure is substituted by the paramagnetic thin film.

The similarity in magnetic saturation and remanence between both samples in Fig. 2 suggests that both samples have the same crystalline texture, i.e., the ϕ grains have the same statistical distribution of orientation. Therefore, we attempt to explain the dramatic annealing temperature dependence of coercivity shown in Fig. 2 as a consequence of the modification of the intergranular region. Our observations strongly suggest that the size as well as the orientation distribution of the ϕ grains, which build up the crystalline structure, remain unchanged during the annealing process.

Let us consider first those samples annealed at the higher temperature range. Since the thickness of the intergranular paramagnetic film is typically of 2.5 nm it is reasonable to assume that the exchange interactions between different grains are negligible.[20] The magnetization curve is expected to behave as the average magnetization curve of the ϕ grains. From Fig. 2 the existence of single and multidomain grains can be derived. The initial part of the magnetization curve characterized by a relative high susceptibility is clearly due to domain-wall motion which takes place in the multidomain grains. When the magnetization approaches 40 emu/g a remarkable decrease of susceptibility is observed. When the applied field reaches a value of 1.8 T the susceptibility increases again indicating that irreversible reversal processes occur in the single-domain grains. For higher fields, close to 3 T, the susceptibility decreases and only reversible rotation processes proceed. Therefore, the volume of the sample consists approximately in 50% of single domain and 50% of multidomain grains.

The behavior of the samples annealed at the low-temperature range is rather different. As is shown in the same Fig. 2 the magnetization process does not exhibit in this case the two well-defined processes. It seems that only multidomain-grain contribution takes place. The difference between the two magnetization curves plotted in the figure can be understood if the presence of small ϕ grains connecting the bigger ones leads to the disappearance of the single-domain contribution.

A simple scheme is outlined in which the effect of exchange interactions between grains with different orientation of easy axes on the magnetization curve is shown.

Let us consider the switching process, at 0 K, of six magnetic moments m, separated a distance l, constant along the x axis, from $x=l$ to $x=6l$. It is assumed that they interact with the uniaxial crystalline field proportionally to D and are exchange coupled through JS^2 (J is the exchange integral and S the spin which gives rise to m, with $m=\mu_B g S$, where μ_B is the Bohr magneton and g the Landé factor). We also assume the easy axis to be the z axis for the six positions of the magnetic moment. The magnetization curve at 0 K of this linear set of magnetic moments is similar to that corresponding to a single domain. In particular when the applied field is acting along the z axis the magnetization curve is an step function centered at the anisotropy field, $H_k=(2D/\mu_0 m)$.

Consider now an extra magnetic moment located at $x=7l$, with the same crystalline field strength but easy axis oriented along the y axis. This seventh magnetic moment is exchange coupled to its first neighbor located at $x=6l$ through γJS^2, where the parameter γ varies between 0 and 1. It is clear that this new magnetic moment corresponds in our analogy to the small ϕ grains observed in the intergranular region of the samples annealed at low temperatures. Let us consider how the presence of this extra magnetic moment can introduce remarkable changes in the magnetization process of the starting single domain (linear set of six magnetic moments). It is also shown that the influence of the extra moment is mainly governed by the value of the intergranular exchange parameter.

Let us suppose that a magnetic field high enough to saturate the linear chain of spins is applied along the positive z axis. When the field is removed the orientation of the magnetic moments can be found by minimizing the magnetic free energy which can be written as

$$F_1=\sum D\,\sin^2(\zeta_i)-\sum JS^2\,\cos(\zeta_{i+1}-\zeta_i) - \gamma JS^2\left[\left(\frac{\pi}{2}\right)-(\zeta_7-\zeta_6)\right], \tag{3}$$

where ζ_i are the angles between m_i and the positive z axis for i ranging between 1 and 6 and ζ_7 the angle between m_7 and the positive y axis.

The magnetic energy of the system changes under the action of a magnetic field acting along the z axis as

$$F=F_1-\sum \mu_0 mH\,\cos(\zeta_i)-\mu_0 mH\,\sin(\zeta_7). \tag{4}$$

Since the mean magnetic moment along the z axis is given by

$$\langle m\rangle=\frac{[\Sigma m\,\cos(\zeta_i)+m\,\sin(\zeta_7)]}{7}, \tag{5}$$

minimization of M as a function of ζ_i in Eq. (4) allows us to find the shape of the hysteresis loop. Figure 6 illustrates the hysteresis loop obtained by numerical calculation of the minimum of F as a function of the parameter γ. Computation was performed by assuming a value $(JS^2/D)=3$, which

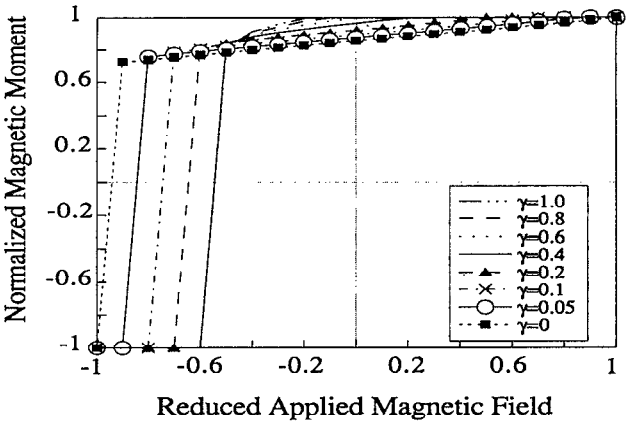

FIG. 6. The dependence of the hysteresis loop, $\langle m\rangle-h$, as a function of γ is shown.

is the approximated value for the exchange to anisotropy ratio of ϕ grains. The field is expressed in terms of the reduced applied field $h=(\mu_0 m/2D)$. It is interesting to note how the presence of the small grain (the magnetic moment located at $x=7l$) affects the coercive field even for low values of the intergranular exchange parameter γ. The coercive field dependence on γ has been plotted in Fig. 7.

V. CONCLUSIONS

It is concluded that homogeneous nucleation occurs previous to crystal growth as the main crystallization mechanism. Further assuming a constant growth rate in the first crystallization steps, a systematic examination of several thinned foils allowed to establish the order of magnitude of both nucleation frequency and crystal growth rate whose values at 795 K are $I=10^{16}$ m^{-3} s^{-1} and $U=10^{-10}$ m s^{-1}. This relatively high nucleation rate promotes a quite refined nanostructure that has an important effect on the magnetic behavior of the material. Samples annealed in the range 755–850 K exhibit an intergranular eutectic nanostructure that melts during subsequent higher temperature heat treatment to form

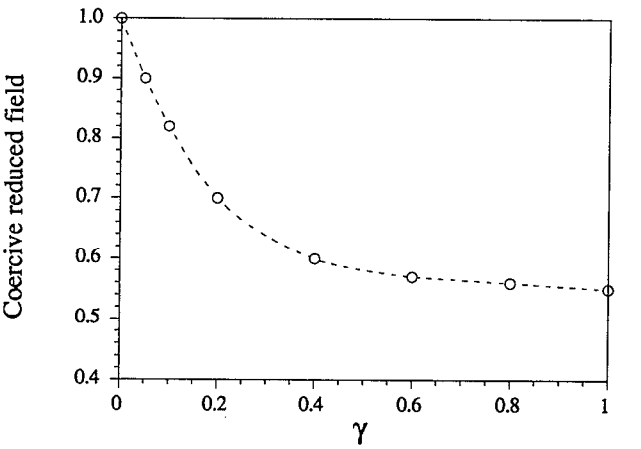

FIG. 7. The coercive reduced field is plotted as a function of γ.

a paramagnetic Nd thin film. A drastic increase in the coercive field from 0.9 to 1.9 T is associated with this evolution of the microstructure.

It has been shown, by using a simple analogy, that the switching magnetization field in a single domain can be drastically affected through the exchange coupling to neighbor grains with different orientation of the easy axis. This effect should be particularly important when trying to enhance the coercive field of polycrystalline hard magnetic materials, as analyzed with some detail elsewhere.[21]

For samples annealed at temperatures between 755 and 850 K the intergranular small grains contact the larger ones. According to the results shown in Fig. 7, when the value of the exchange between the small and big grains is about 0.2 times the value of the intergranular exchange coupling the coercive field can be reduced a factor 0.6 respect to the value expected when the big grain is exchange isolated. Exchange isolation condition is almost perfectly reached in the samples annealed at high temperatures. For this case it seems likely that the presence of the paramagnetic film between the ϕ grains eliminates or reduces the possibilities of intergranular exchange, so giving rise to an increase of the coercive field.

ACKNOWLEDGMENTS

Authors wish to thank Dr. P. Crespo and I. Navarro for their collaboration in the preparation of the manuscript. This work was partially supported by the Comisión Interministerial de Ciencia y Tecnología, CICYT (Projects No. MAT91-0907, No. MAT92-0491, and No. MAT92-0405), which assistance is acknowledged.

[1] J. Wecker and L. Schultz, J. Appl. Phys. **62**, 990 (1987).
[2] J. J. Croat, J. F. Herbst, R. W. Lee, and F. E. Pinkerton, Appl. Phys. Lett. **44**, 148 (1984); **55**, 2078 (1984).
[3] G. E. Carr, H. A. Davies, and R. A. Buckley, Mater. Sci. Eng. **99**, 147 (1988).
[4] Kh. Ya. Mulyukov, R. Z. Valiev, G. F. Korznikova, and V. V. Stolyarov, Phys. Status Solidi A **112**, 137 (1989).
[5] A. Jha, R. A. Buckley, and H. A. Davies, J. Magn. Magn. Mater. **80**, 109 (1989).
[6] G.-H. Tu, Z. Altounian, D. H. Ryan, and J. O. Strön-Olsen, J. Appl. Phys. **63**, 3330 (1988).
[7] M. T. Clavaguera-Mora, M. D. Baró, S. Surinach, and N. Clavaguera, J. Mater. Res. **5**, 1201 (1990).
[8] R. W. Lee, Appl. Phys. Lett. **46**, 790 (1985).
[9] R. W. Lee, N. Schaffel, and L. Brewer, IEEE Trans. Magn. **MAG-21**, 1958 (1985).
[10] J. Wecker and L. Schultz, J. Appl. Phys. **62**, 990 (1987).
[11] S.-I. Hatta and T. Mizoguchi, Jpn. J. Appl. Phys. **27**, 597 (1988).
[12] P. J. Grundy, D. G. Lord, S. F. H. Parker, and R. J. Pollard, in *Concerted European Action on Magnets (CEAM)*, edited by I. V. Mitchell, J. M. D. Coey, D. Givord, I. R. Harris, and R. Hanitsch (Elsevier, Amsterdam, 1989).
[13] J. A. Diego, M. T. Clavaguera-Mora, and N. Clavaguera, Mater. Sci. Eng. (to be published).
[14] M. T. Clavaguera-Mora, J. A. Diego, M. D. Baró, S. Surinach, A. Hernando, P. Crespo, and G. Rivero, J. Magn. Magn. Mater. **119**, 289 (1993).
[15] J. Fidler and K. G. Knoch, J. Magn. Magn. Mater. **80**, 48 (1989).
[16] R. K. Mishra, J. Magn. Magn. Mater. **54–57**, 450 (1986).
[17] N. Clavaguera and J. A. Diego, Intermetallics **1**, 187 (1993).
[18] G. Schneider, E. T. Henig, B. Grief, and G. Knoch, Z. Metallkd. **77**, 1755 (1986).
[19] W. Kurtz and D. J. Fisher, in *Fundamentals of Solidification* (Trans. Tech, Zürich, 1986).
[20] N. García and A. Hernando, J. Magn. Magn. Mater. **99**, L12 (1991).
[21] A. Hernando, J. Magn. Magn. Mater. **117**, 154 (1992).